Reactivity descriptors for ceria in catalysis

Marçal Capdevila-Cortada,[a] Gianvito Vilé,[b] Detre Teschner,[c,*] Javier Pérez-Ramírez,[b,*] Núria López [a,*]

(a) Institute of Chemical Research of Catalonia (ICIQ), The Barcelona Institute of Science and Technology, Av. Països Catalans 16, 43007 Tarragona, Spain; (b) Institute for Chemical and Bioengineering, Department of Chemistry and Applied Biosciences, ETH Zurich, Vladimir-Prelog-Weg 1, 8093 Zurich, Switzerland; (c) Fritz-Haber-Institute of the Max Planck Society, Faradayweg 4-6, 14195 Berlin, Germany.

E-mail: teschner@fhi-berlin.mpi.de; jpr@chem.ethz.ch; nlopez@iciq.es

Keywords: Ceria; structure-activity relationships; oxidation; hydrogenation; acid-base; redox.

Highlights:

- The catalytic performance of ceria has been systematized in terms of chemical descriptors.
- Basicity and redox properties contribute simultaneously to several catalytic phenomena.
- Experimental rates can be quantitatively expressed by combinations of the chemical descriptors.
- These chemical descriptors can be extended to other oxides.

ABSTRACT

Ceria has been very successfully employed in oxidation catalysis, whereas its application in other reactions has been less intensively investigated. The catalytic activity of ceria can be further enhanced by the use of dopants, and it exhibits structure sensitivity for numerous processes. The rich chemistry of cerium oxide is gathered and discussed in the present work, where the nature of each step of the most common reactions performed on it is assessed. Chemically intuitive computational and experimental descriptors, namely acid-base, redox, and structural features, are put forward to correlate the observed trends among the different doped and undoped facets. We have attempted to generate a robust framework that maps the chemically sound descriptors to the experimental fingerprints and theoretically calculated parameters.

1. Introduction

Ceria has reached an iconic status among binary oxides, as it keeps more secrets than any other due to the versatile chemical structure, in addition to the fact that although being a rare earth it is abundant and relatively cheap [1]. Ceria is an excellent playground to understand complex chemistry, as (i) it shows marked structure sensitive properties [2], which can be nowadays assessed through shape controlled synthesis [3–5]; (ii) it shows both acid-base and redox chemistry [6,7]; (iii) it presents oxygen transport properties [8,9]; (iv) it is stable under harsh conditions [10]; (v) it is relatively easy to modify by doping to improve its chemistry [11,12]; (vi) it presents interesting hydrophobic features [13,14]; and (vii) it also exhibits a complex electronic structure that makes modeling efforts challenging [15,16]. All these characteristics make ceria as a unique material with fascinating properties and a wide scope of applications in heterogeneous catalysis [1,17].

The exploitation of the catalytic and chemical properties of CeO_2 has been commonly based on its oxygen storage capacity, OSC [11,15,18,19]. A good OSC material requires a few contributions: (i) the cycling between the oxidized and reduced forms is energetically not demanding (or, equivalently, it presents low vacancy formation energy); (ii) easy transport of the vacancies (O atoms) between the surface and the bulk and inside the bulk; and (iii) facile transformation between the crystal structures of the oxidized (CeO_2) and reduced (Ce_2O_3) forms or, at least, facile alignment of vacancies through defect lines. The OSC has been instrumental to understand the chemistry, either as a catalyst or a support, in many oxidation processes [7,19]. Due to its OSC, ceria is also employed as a ceramic electrolyte in solid oxide fuel cells, typically doped with aliovalent cations [20–23].

Since the identification of these properties, numerous reactions based on the high oxidation ability of ceria-based materials have been put forward. For instance, CeO_2 can oxidize CO and soot, especially at medium temperatures, and thus it is incorporated in three-way catalysts in combination with metallic nanoparticles [7,19]. Ceria also performs nicely in the preferential oxidation (PROX) of CO in CO:H_2 mixtures [24–26]. This reaction is required to clean H_2 feeds from impurities that can damage fuel cells if H_2 is employed as an energy vector. In addition, it can also drive the water-gas shift reaction, i.e. the production of CO_2 and hydrogen from a mixture of CO and water, thus improving the hydrogen content in syngas mixtures [26–28]. Furthermore, oxidation properties can be extended to the application in the Deacon process [29]. This reaction aims at the recycling of hydrogen chloride by employing the following process $4HCl+O_2 \rightarrow 2Cl_2+2H_2O$. The reaction can be seen as an oxidation and thus close to the traditional uses of CeO_2, but at the same time the competition of Cl and O for the same type of sites limits the application of the common descriptors for oxidation processes [10,30–33]. Still, limiting the catalytic properties of ceria to its use in oxidation is far a simplistic identification, as it was recently shown to promote the semi-hydrogenation of alkynes to alkenes under hydrogen-rich conditions [34–36]. The

description of this catalytic versatility sets a new landmark in the research of these materials.

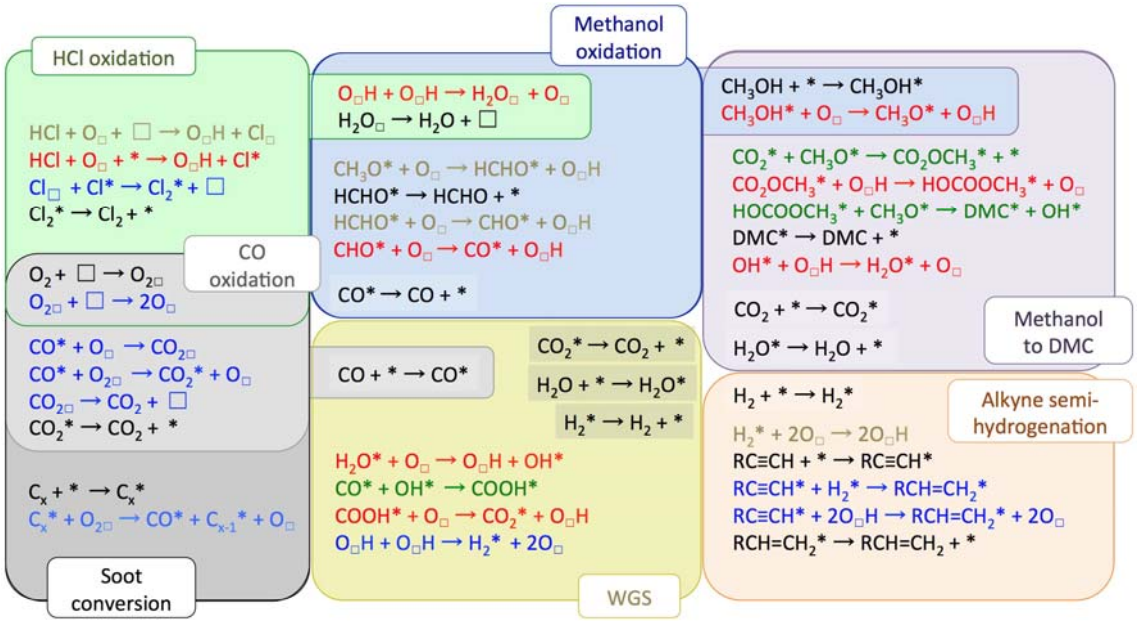

Fig. 1. Schematic representation of the sets of frequent applications of CeO_2 in catalysis, manifesting common steps in the reaction networks. The related inverse steps are also highlighted. The colors of the reactions correspond to Brønsted acid-base (red), Lewis acid-base (black), redox (blue), combined acid-base redox (brown), and condensation (green) steps. For more details see the corresponding sections below.

Perhaps not so widespread but still largely studied are other reactions performed over ceria, mostly involving simple or polyfunctional organic molecules. The conversion of alcohols, e.g. methanol [37–41], ethanol [42,43], or polyols [44–46], has been carried out on ceria, as well as other organic compounds [47–51]. Methanol is also used in the conversion of CO_2 to dimethyl carbonate (DMC) catalyzed by ceria [52–55]. Finally, NO_x [56–58], SO_x [59–64], and H_2S [65–67] react on ceria leading to either oxidized or reduced products depending on the reactant and the exposed ceria surface.

Fig. 1 illustrates the intricate map of the most common reactions catalyzed by CeO_2. The links between the different steps and the identification of the chemical nature of each step are also shown. A coherent systematization of the catalytic properties of ceria has not been yet undertaken, although many authors have pointed out the need of separating the different terms as acid/base, redox, or condensation [68–73]. Our aim in this article is to revise these applications and to identify the principles that guide the performance of CeO_2 in catalysis. For this purpose, a set of activity and selectivity descriptors both for oxidations and hydrogenations are presented, and the detailed analysis is then applied to describe: (i) a set of relevant reactions; (ii) several facets that account for the strong structure sensitivity observed; and (iii) the effect of introducing dopant cations on the different properties. This integrative perspective identifies the descriptors and maps them to direct observables accessible from experiments.

2. Descriptors for ceria

2.1. Previous descriptor-based oxidative chemistry

Structure-performance relationships are crucial to rationalize catalytic phenomena [74–76]. Typically, if the rate, selectivity, or stability correlate with a single parameter or a group of parameters these are taken as descriptors, as they can express the activity summarizing all the information for a class of materials. Energy descriptors have been extensively used since the work of Sabatier [77], and are nowadays accepted as the most robust theoretical tools in high-throughput computational screening of materials. Reactions become even more complex on oxides, and thus the assessment of their catalytic performance requires also more complex descriptors. In particular, to describe the activity and selectivity of oxides, especially in oxidation processes, seven pillars were postulated in the pioneering work by Grasselli [78]: host structure, redox, metal-oxygen bond, lattice oxygen, phase cooperation, multifunctionality of active sites, and site isolation, as illustrated in **Fig. 2**. These pillars, despite providing clear conceptual guidelines, are described in a qualitative manner and can hardly be mapped directly to particular fingerprints in experiments. Thus, this list may be considered as a set of general principles, rather than quantitative parameters that can be adjusted to reach the desired reactivity. Furthermore, some pillars are not orthogonal and hence they cannot be individually tailored, hindering the direct interpretation of the described chemical process.

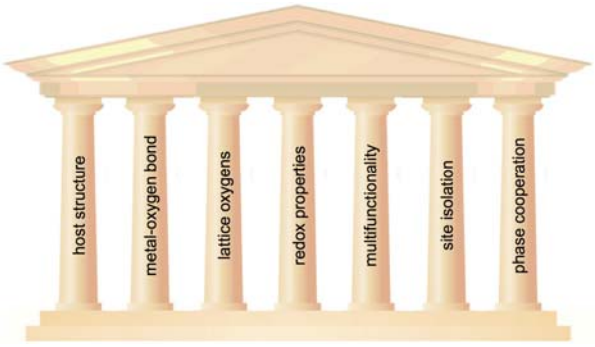

Fig. 2. Schematic illustration of Grasselli's seven pillars, based on ref. [78]. Notice that although the pillars seem parallel, the descriptors overlap to some degree.

The oxygen vacancy formation energy has been commonly taken as the primary, and sometimes unique, descriptor for reactivity in computational approaches, restricting the pillars into a single property. However, not all reaction schemes involving vacancy formation can be described with this single magnitude, especially for reaction environments where the surface structure differs significantly from the pristine surface [31]. Moreover, hydrogenation reactions do not entail vacancy formation, presenting a complementary set of governing factors and complex steps that couple acid-base and redox properties.

Although the correspondence between the pillars and experimental or computational descriptors is not one-to-one, the concepts described in the oxidation chemistry by Grasselli are fully expanded in **Table 1**. In addition, one must keep in mind that the state of the surface under reaction conditions is usually very particular in terms of stoichiometry, configuration, electronic structure, etc. Descriptors have been traditionally proposed to describe the pristine surface, instead of the catalyst state under working conditions, and thus they might be irrelevant to the activity if they are not self-consistently analyzed.

Table 1. Experimental and theoretical mapping of the seven pillars suggested by Grasselli. The abbreviations used can be found in the text.

Pillar	**Property**	**Experimental technique**	**Computational descriptor**
Host structure	Tridimensional structure	XRD, neutron scattering	Distances, topology
	Local coordination	EXAFS, STM	Local coordination
M-O bond	Energy	Raman	Cohesive energy Vacancy formation energy
	Geometric	EXAFS	Geometry
Redox		TPR, XPS, UPS, EPR cyclic voltammetry	Ionization potential Electron affinity
Lattice oxygen	Vacancy formation	OSC	Vacancy formation energy
	Diffusion	OSC	E_a diffusion
	Basicity	TPD (CO_2)+IR	O_{2p}, E_{CO2}
	M-related Acidity	TPD (CO, NH_3)	E_{CO}
Site isolation		Selectivity assessment by catalytic testing [a]	Lateral interactions
Multifunctionality of active sites		TPD of multifunctionalized molecules, FTIR of probe molecules	Adsorption energy for different configurations sampling sites Acid-base/geometry Descriptor combinations
Phase cooperation	Different phases	XRD	Equilibrium diagrams
	Uptake	PGAA	Resting state first principles thermodynamics

[a] Site isolation at the catalytic surfaces might be proposed based on selectivity assessment in partial hydrogenation and oxidation reactions.

2.2. Chemical descriptors: mapping between experiments and theory

In the following paragraphs we present an alternative descriptor-based formulation, which can be translated into the pillars. The suggested descriptors are quantified contributions retrievable often from both calculations and experiments, which can be typically classified as electronic or geometric. However, the sparse

characterization derived from experiments, especially related to probe molecules (formation of undesired species, dissociation, adsorption in multiple sites, etc.), advocates the use of first-principles calculated descriptors, given their easier control of the single desired property.

The electronic descriptors include:

The **charges** associated to the surface atoms (q_O, q_{Ce}). Oxides present charge separation so that the first interaction between a molecule and the surface is the electric field generated by the point charge distribution. We have computationally obtained them from a Bader analysis [79]. However, charges are not observables and hence they cannot be retrieved from experiments. The spin-polarized density, on the other hand, is an observable that can be measured by electron paramagnetic resonance (EPR) spectroscopy, and sometimes might correlate with the charges.

The **basicity** of the surface anions (O_{2p}), which has two main contributions: the total charge (as defined above) and the levels alignment with respect to the adsorbate, or, alternatively, to the Fermi level, which would correspond to how available (polarizable) are the oxygen lone pairs to share their density. These definitions include both Brønsted and Lewis basicity. The basicity term can be traced back from temperature programmed desorption (TPD) peaks of probe compounds or from shifts in their vibrational spectra. Equations that link the TPD peaks to adsorption energies can be used with this purpose [80]. Computationally it is obtained by their adsorption energy or, alternatively, as the center weighted average in the projected density of states (PDOS) of the surface oxygen 2p band. The Lewis **acidity** of the cation centers (E_{CO}) can be determined in a similar manner, using CO or NH_3 as probe molecules [81]. Yet, another point regards to the presence of hydroxyl groups on the surface, which correspond to Brønsted acid sites. Experimentally, the degree of control of the surface hydroxyl groups is a crucial parameter that depends on the sample preparation and activation. However, this is typically not considered in theoretical simulations, as the clean surface is taken as the common initial structure.

The **redox** term (E_{red}), which for the particular case of ceria is based on the ability of the cations to accept one electron [82]. This term is related to the OSC and can be obtained from experiments, but it should not be considered as a standalone E_{red} contribution. The E_{red} term is computationally obtained by adding one extra electron to the unit cell, ensuring the proper localization [83]. Notice that this is equivalent to the reduction potentials associated to the half-reaction of the total redox process. It is worth noting that whenever aliovalent dopants are present, hole or particle states appear. This may drastically change the E_{red} contribution, especially for hole states generated within the band gap. The hole/particle states can be identified by their charge, electron density, and the corresponding energy.

The geometric terms related to the host structure contain:

The **distances** between surface atoms ($d_{i,j}$, where i and j are atoms in the lattice). Distances are related to the bulk structure and, for the most common terminations, surface effects do not alter them significantly. Dopants might induce uneven and sharp expansions/contractions, the higher the difference is in the radii of the parent and dopant atoms, the larger this volume change.

The **local coordination** of surface anions and cations (N_O, N_{Ce}). This term can be retrieved from experiments by scanning tunneling microscopy (STM) or extended X-ray absorption fine structure (EXAFS). Structure sensitivity is typically a direct consequence of the changes in the distances or the coordination patterns. Notice that, in some cases such as polar surfaces (e.g. the (100) facet of ceria), the fraction of intrinsic vacancies, $x_{\square}$, due to surface reconstruction will have a major impact on the local coordination.

The previous two properties and the symmetry patterns can be combined into the term **ensemble**, this is the geometry of the active site. On oxides, these effects are typically linked to multifunctional positions, where both contributions from the anion and the cation exist and are linked to their relative topology.

Two final aspects discussed by Grasselli are **phase cooperation** and **site isolation**. The former term was said to appear when the key catalytic functions cannot be incorporated into one single catalytic phase, and thus two or more phases are required in close proximity. The appearance of different phases upon reaction is typically reported by X-ray diffraction (XRD). In some cases, the tridimensional structure does not change but the material takes some of the reactants up, converting a pure oxide phase for instance into an oxyhalide, as seen for the oxidation of hydrogen halides by operando prompt gamma-ray activation analysis (PGAA). In a broader sense, reaction fronts on metals might be seen as phase cooperation, where under some conditions the reaction takes place in areas where two different compounds or surface states are in close proximity [84,85]. This has been found to a certain extent in theoretical simulations, where the areas of maximum activity are linked to positions where the two reactants are more likely to be mixed [86,87]. An alternative phase cooperation can be found for ceria supported metal catalysts, where bifunctional mechanism with one part of the reaction network taking place on the metal and another set of reactions occurring in the oxide would also belong to this category. Site isolation contributions are typically crucial to assess selectivity as they govern the activity of the sites. It can be experimentally inferred by either analyzing side products in catalytic tests or performing adsorption tests of molecules that simultaneously probe two centers. Computationally, it can usually be described as a combination of the coordination number and the surface distances mentioned above. The descriptors corresponding to phase cooperation and site isolation will be only briefly touched upon in the present work.

Additionally, the **oxygen vacancy formation energy** ($E_{\square}$) has been usually considered as the simplest descriptor for the activity of ceria-based catalysts, as

previously stated. We have therefore included it in our approach. Vacancy formation leaves two electrons in the hole left by oxygen removal, which must be accommodated by the surface [88]. In ceria, the electrons are hosted by the reducible cations, which tend to be localized in the next-nearest neighbors to the vacancy [89]. This induces lattice distortions due to the larger radius of the Ce^{3+} cations. The vacancy formation energy is obtained from calculations as $E_{\square} = E(CeO_{2-x}) + 1/2E(O_2) - E(CeO_2)$.

An alternative descriptor related to oxygen vacancies is the experimental **oxygen storage capacity** (OSC). This magnitude is related to the formation of oxygen vacancies and their diffusion in the material toward/from the surface. The OSC is measured as the weight loss of the sample due to oxygen removal, commonly using CO or H_2, and it depends on the history of the sample (i.e. on how the sample was prepared and its subsequent treatments). Therefore, the sample can be tailored to reach desired OSC values. However, the experimental measurements strongly depend on the protocols applied, and thus reproducibility requires very strict degree of control and a strict standardization in order to compare data among laboratories. The computational assessment of the OSC is much more complex. In principle, an extensive investigation for the equilibrium oxygen loss could be done by coupling DFT to the environment through first-principles thermodynamics [90]. However, the intrinsic approximations included in the latter methodology prevent from obtaining quantitative correct values even for the equilibrium oxygen vacancies [91].

Finally, it is worth noting that the state of the surface, in particular under reaction conditions, could affect both the pillars and the descriptors. The analysis presented here is devoted to the evaluation of the clean or slightly modified surface, i.e. not allowing large coverage effects or significant surface reconstructions. Coverage effects, however, might influence the values of the descriptors to a large extent. Nevertheless, our aim in this work is to present the proof of concept of the methodology, and this is easier to carry out under clean surface conditions. Coverage-dependent descriptors, for the most common coverage situations, could be introduced in a simple yet efficient manner to study the role of coadsorbates on the reactivity. Furthermore, the only surface defects considered in this study are point defects, namely oxygen vacancies and dopant cations. Other defects such as steps or low-coordinated centers (e.g. edges or corners) are not considered, given the relatively large nanoparticles on which the following reactions are typically performed. Low-coordinated sites can however be treated in the same methodology described here.

Descriptors are related to the characteristics of the particular reaction networks. Therefore, a detailed knowledge of the elementary steps provides an easier identification. In the following, we have employed reaction networks reported in the literature, exception made for the DMC synthesis case, where a potential reaction network is proposed. The main reaction pathways in complex reaction networks depend on the reaction conditions, which affect the relative stability of the difference phases and in some cases the dynamics of these phases. From a theoretical point of view, these phases need to be evaluated separately and if they cooperate then the model shall

include the boundary. In the cases studied herein, ceria maintains its properties unless indicated (halide uptake).

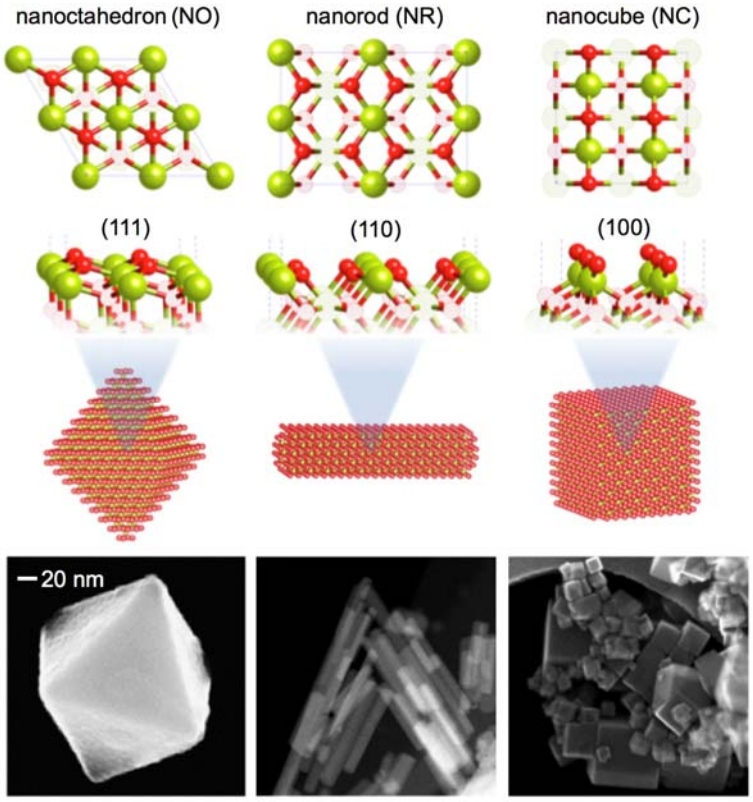

Fig. 3. Structure and composition of ceria nanoctahedra (left), nanorods (middle), and nanocubes (right). The micrograph of ceria nanoctahedra is adapted from [92]. Color codes: O (red) and Ce (yellow).

2.3. Descriptors for cerium oxide reactivity

Most of the reactions discussed in this work are performed over ceria nanoparticles, **Fig. 3**, although some examples over extended films are also examined. The (111) termination is the most stable ceria surface, and it is the exposed facet of well-defined ceria nanoctahedra. In addition to this nanoshape, ceria nanorods and nanocubes are also routinely synthesized [3–5]. The former mainly expose (110) facets, with (100) and (111) to a lesser extent, whereas the latter present (100) termination planes. The (100) surface is polar and thus requires polarity compensation reconstruction that may lead to Ce- or O-terminations [93]. Commonly the latter termination is considered the most stable (100) reconstruction and thus it is the one assumed in this study [94–98]. Although the environment might particularly affect polar surfaces, where adsorbates can promote certain reconstructions [99,100], we have limited our approach to the pristine oxygen terminated reconstruction. It is worth noting that the different exposed facets are of particular importance given the structure sensitivity observed for many processes [2].

The descriptors listed in the previous section are collected in **Table 2**, for the (111), (110), and (100) ceria surfaces. The most direct descriptor is the local coordination of the topmost cerium and oxygen atoms. The (111) surface presents higher coordination for both atoms, N_{Ce} = 7 and N_O = 3, whereas the former decreases to 6 in both (110) and (100), and N_O lowers to 2 in the (100), but remains 3 in the (110). A straight consequence of N_O is the Ce-O distance ($d_{Ce,O}$), which experiences a minor difference between the (111) and the (110) surfaces but decreases significantly on the (100) facet. The $d_{O,O}$, on the other hand, is equivalent in the (111) and (100) surfaces, but two shorter distances exist in the (110) as a result of the morphology of this termination plane (**Fig. 3**). Although the charges of surface Ce and O do not change significantly, the other electronic descriptors show more drastic differences among the surfaces. The basicity term is much higher and nearly identical for the (111) and (100), and lower for the (110) surface. However, the acidity of the cerium atoms increases following the order (100) > (110) > (111), inverse to their stability order. The E_{red} term is endothermic in all cases, being 0.65 and 1.65 eV for the (111) and (110), respectively, and almost zero for the (100). This parameter is completely connected to how the surface can accommodate the bigger Ce^{3+} cations. The low N_{Ce} and N_O coordinations in (100) favor the required rearrangement to incorporate the Ce^{3+}. However, in the (110) surface, since each Ce^{4+} is surrounded by four O in the surface plane (**Fig. 3**), the accommodation of the bigger reduced atom is less favored. Finally, the endothermic vacancy formation energy is higher for the (111), followed by the (100) and the (110) surfaces. The latter termination further stabilizes the vacancy formation by bridging an oxygen atom between two cerium cations as a split vacancy [101,102]. It is worth noting that on the (111) surface, the lowest vacancy formation energy corresponds to the subsurface vacancy [15], whereas this is not the case for the other two low-index surfaces. Notice also that since the (100) is a polar surface, reconstruction is required to compensate the polarity and render it stable [93,103]. Such reconstruction leaves a fraction of 0.5 of intrinsic oxygen vacancies, $x_{\square}$ [104]. This fact also enables the surface to adsorb oxygen atoms on these vacancy sites, which is an endothermic process but still more favorable than vacancy formation.

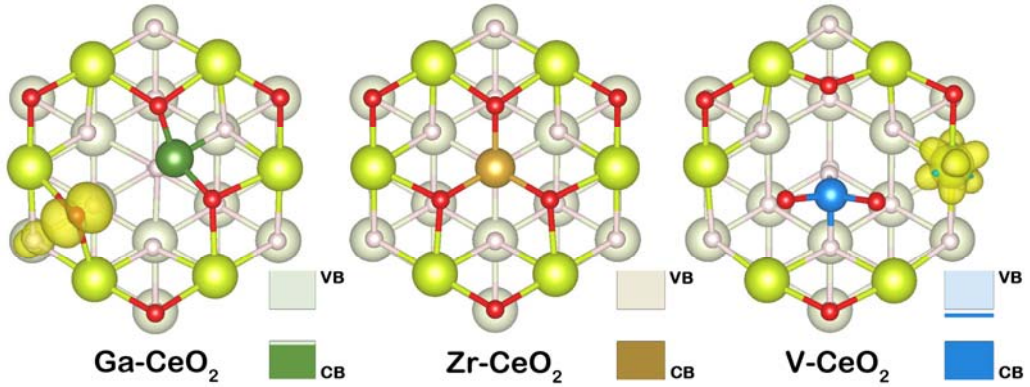

Fig. 4. Electron localization of holes or particles in Ga-, Zr-, and V-doped ceria(111). The small insets illustrate the resulting band structure for each doped surface, where the hole in the conduction band and the particle in the band gap close to the valence band are qualitatively shown for the Ga- and V-CeO_2 materials, respectively.

Similar to **Table 2**, **Table 3** contains the descriptor values for Ga-, Zr-, and V-doped ceria(111). Ga- and V-CeO_2(111) are examples of aliovalent dopants (n- and p-type, respectively), whereas Zr-CeO_2(111) is an example of isovalent doping, **Fig. 4**. The addition of dopant cations induces symmetry breaking, which drastically influences some specific descriptor values. On the one hand, cerium and oxygen charges, local coordinations, and surface acidity remain almost unaltered. On the other hand, doping has severe impact in interatomic distances, oxygen basicity, redox, and vacancy formation energy. The average $d_{Ce,O}$ and $d_{O,O}$ distances are almost not influenced, but the values close the dopant site can vary for $d_{Ce,O}$ ca. 0.1, 0.05, and 0.3 Å for Ga-, Zr-, and V-ceria, respectively, and ca. 0.5, 0.4, and 1.1 Å, respectively, for $d_{O,O}$. The basicity term decreases for the three doped surfaces compared to the pristine CeO_2(111), strongly on the p-doped surface. The addition of n- or p-type dopants triggers a singular change on the electronic structure of the semiconductor material, creating a hole or a particle state, respectively. This has major consequences on E_{red} and $E_{\square}$ terms. Although for Zr-CeO_2(111) both descriptors decrease in a notable manner, for Ga- and V-CeO_2(111) this decrease is much larger, and E_{red} is even highly exothermic for the n-doped surface. Interestingly, subsurface vacancy formation is still favorable for the isovalent doping, but turns unfavorable for Ga- and V-doping.

The descriptors listed in Tables 2 and 3 will serve as the framework to describe the most common reactions performed on ceria. The computational set up for the calculations is summarized in the Supplementary Material, while the details on the experiments can be found on the particular references. Nevertheless, this list enables us to start providing a quantitative description of the most recurrent term related to the reactivity on ceria, the vacancy formation energy, based on the systems previously detailed, which include the three pristine and the three doped surfaces. The vacancy formation energy is found to be a combined balanced function of the basicity of the surface oxygens and the redox ability of the surface, O_{2p} and E_{red} (**Fig. 5**). Therefore, $E_{\square}$ depends simultaneously on the stability of the surface oxygen and on how well the surface can accommodate the electrons left by the oxygen removal. Both descriptors are individually unable to correlate $E_{\square}$, however their combination results in a collective descriptor that provides a notable description of the vacancy formation energy. In particular, the relative weigh of each variable in the collective descriptor is 0.58 for E_{red} and 0.42 for O_{2p}, once balanced by the span of each variable (E_{red} and O_{2p} span 2.12 and 0.52 eV, respectively, see Tables 2 and 3).

Collective descriptors are sometimes crucial to describe certain complex steps or adsorptions [105–108]. These descriptors are not observables and do not have an additional physical meaning other than the proper balance of the individual contributions. It is also worth noting that the coefficients of each variable may be expressed in the right units to correctly describe the correlated magnitude.

Table 2. General descriptors for the lowest surface energy facets of CeO_2. The charges are in $|e^-|$, distances in Å, and energies in eV (negative values correspond to exothermic processes).

		(111)		(110)		(100)	
		Calc.	Exp.	Calc.	Exp.	Calc.	Exp.
N_{Ce}	first neighbors	7	-	6	-	6	-
N_O	first neighbors	3	-	3	-	2	-
$d_{Ce,O}$	metal-oxygen distances	2.375	-	2.342	-	2.206	-
$d_{O,O}$	oxygen-oxygen distances	3.886	-	2.604 2.898 3.887	-	3.887	-
q_{Ce}	ion charge	2.37	-	2.31	-	2.33	-
q_O	ion charge	-1.19	-	-1.16	-	-1.12	-
O_{2p}	oxygen basicity	-0.95	0.1 [a]	-1.45	0.9 [a]	-0.93	0.3 [a]
E_{CO}	CO adsorption	-0.19	w [b]	-0.24	w [b]	-0.34	w [b]
E_{red}	surface reduction	0.65	-	1.16	-	0.03	-
$E_{\square}$	vacancy formation energy surface	1.85	-	1.17	-	1.57 (0.99) [c]	-
$E_{\square, ss}$	vacancy formation energy subsurface	1.68	-	2.22	-	3.21	-
OSC	oxygen storage capacity	-	318 [d] 0.4 [e]	-	554 [d] 6.3 [e]	-	353 [d] 6.8 [e]
$x_{\square}$	intrinsic defective fraction	0	-	0	-	0.5	-
ρ_{spin}	spin density	0	-	0	-	0	-

[a] CO_2 adsorption rate (in CO_2 nm^{-2}), from [71]. [b] w = weak, from [71]. [c] In parentheses: energy requirement upon the addition of an oxygen atom to the stoichiometric surface. [d] In μmoles O g^{-1}, from [109]. [e] In μmoles O m^{-2}, from [110].

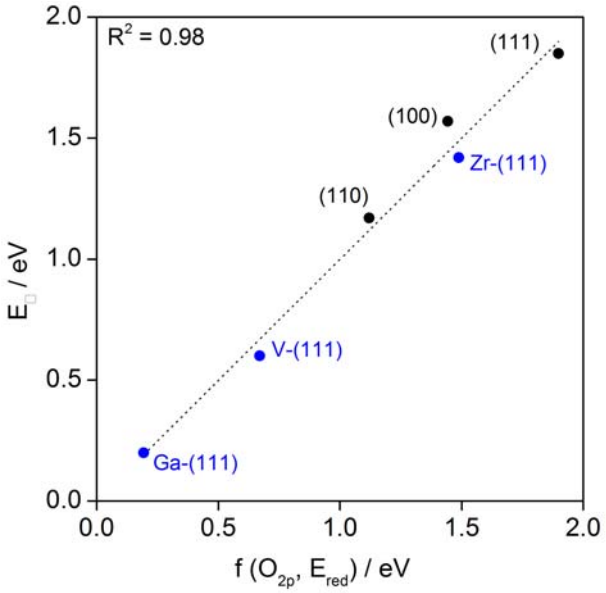

Fig. 5. Dependence of the vacancy formation energy, $E_{\square}$, on a collective variable including the O_{2p} and E_{red} terms, for the pristine (111), (110), (100), and doped Ga-, Zr-, V-(111) ceria surfaces. The fitted equation is $f(O_{2p}, E_{red}) = (2.33\ O_{2p} + 0.78\ E_{red} + 3.60)$ eV.

Table 3. General descriptors for p-, isovalently-, and n- doped CeO_2(111) surfaces, following the nomenclature given in Table 2. The charges are in $|e^-|$, distances in Å, and energies in eV (negative values correspond to exothermic processes). Distance values refer to minimum, average, and maximum distance, respectively.

	Ga-CeO_2(111)	Zr-CeO_2(111)	V-CeO_2(111)
N_{Ce}	7	7	7
N_M	4	4	4
N_O	3 [a]	3	3 [a]
$d_{Ce,O}$	2.277 / 2.379 / 2.519	2.344 / 2.399 / 2.455	2.145 / 2.417 / 2.840
$d_{M,O}$	1.940	2.135	1.715
$d_{O,O}$	3.345 / 3.892 / 4.434	3.469 / 3.883 / 4.106	2.890 / 3.911 / 4.489
q_{Ce}	2.38	2.39	2.34
q_M	1.62	2.51	1.89
q_O	-1.14	-1.20	-1.13
O_{2p}	-1.14	-1.04	-1.26
E_{CO} on Ce	-0.22	-0.22	-0.21
E_{CO} on M	-0.04	-0.12	-0.05
E_{red}	-0.96	0.40	0.01
$E_{\square}$	0.20	1.42	0.60
$E_{\square, ss}$	0.29	1.30	0.97
$x_{\square}$	0	0	0
ρ_{spin}	1.0 ($O^{\bullet}$)	0	1.0 (Ce^{3+})

[a] One of the surface oxygens adjacent to the dopant site has coordination 2.

3. Catalytic applications of ceria

3.1. CO oxidation and water-gas shift reaction

The simplest reaction that has been studied over CeO_2 is CO oxidation [69,111]. Notice that ceria is also a suitable material for soot oxidation, which shares some of the characteristics of the CO oxidation scheme [110]. This reaction can be described based on the following list of elementary steps, where * stands for the Lewis center and □ represents the defect site:

$$O_2 + \square \rightarrow O_{2\square} \quad (1)$$
$$O_{2\square} + \square \rightarrow 2O_{\square} \quad (2)$$
$$CO + * \rightarrow CO* \quad (3)$$
$$CO* + O_{2\square} \rightarrow CO_2* + O_{\square} \quad (4)$$
$$CO* + O_{\square} \rightarrow CO_{2\square} \quad (5)$$
$$CO_2* \rightarrow CO_2 + * \quad (6)$$
$$CO_{2\square} \rightarrow CO_2 + \square \quad (7)$$

Two types of active sites are required. In fact, CO adsorption takes place on the Lewis acid centers of the ceria surface, the Ce^{4+} sites. In parallel, O_2 does not adsorb on the clean surface (**Table 4**), since the electron transfer to O_2 is not favored but only on very particular sites of the surface, i.e. oxygen vacancies, line defects such as steps, and open surfaces like CeO_2(100), which are intrinsically defective.

Vacancies are thus required to perform CO oxidation. Therefore, the vacancy formation energy ($E_{\square}$) and the number of potential adsorption sites (number of vacancies, $x_{\square}$) are the most important activity descriptors. Thus, analogously, CO oxidation activity will depend on the E_{red} and O_{2p} terms, as outlined in **Fig. 5**. Based on this interpretation, the CO oxidation rate is face sensitive over ceria. Considering that the vacancy formation energy varies in the order 110 > 100 > 111, the oxidation rate is expected to follow the trend $r_{110} > r_{100} > r_{111}$. This theoretical activity trend is in line with the experimental findings [69,111,112], where it has been shown that ceria nanocubes are more active in CO oxidation compared to ceria nanooctahedra, **Fig. 6a**. It is worth noting that the large number of basic surface sites on CeO_2 can react with CO and CO_2 molecules, forming carbonates that behave as spectators on the surface [69,113,114]. The presence of unidentate, bidentate, and bridged carbonates has been demonstrated by infrared spectroscopy [69,115].

Ceria octahedra and cubes exhibit a different behavior upon aging [112]. Whereas the nanocubes do not decrease their CO oxidation performance, the aged octahedra are nearly inactive, **Fig. 6a**. As shown in **Table 4**, O_2 only adsorbs on the defective sites of ceria. Therefore, once CO reacts with the adsorbed O_2 filling the vacancy, eq. (4), the reaction can only proceed via (5), which is highly disfavored, especially on the (111) facet. Step (5) is thus described by the $E_{\square}$ term. On the other hand, carbonate formation upon CO adsorption takes place on the (110) and (100) surfaces, and releases two Ce^{3+}. O_2 adsorbs on the Ce^{3+} centers [116–118] that now are extensively available, so the reaction can proceed as in (4). This is however not possible on the (111) surface, since carbonate formation is energetically disfavored on this facet.

Accordingly, doped ceria may enhance CO oxidation by decreasing the vacancy formation energy. Zr-doped cerium oxide increases the OSC, **Fig. 6b**, leading to an increased CO conversion [119]. This is further improved by the use of trivalent dopants, where $E_{\square}$ is significantly diminished [120].

Finally, various metal nanoparticles supported on ceria exhibit high CO oxidation activity, namely Au, Cu, Pt, or Pd [26,121–129]. **Fig. 6c** shows how CO conversion is enhanced on Au/CeO_2 compared to pristine CeO_2. Oxides with metal supported clusters are a paramount example of phase cooperation, where the oxide and metal phases can promote different steps of the mechanism [27]. Some steps are thermodynamically favored via oxygen spillover from ceria to the metal [130]. Plenty of studies have been conducted on metal-supported ceria catalysts, but our analysis focuses on standalone ceria, and hence, these are beyond the scope of this work.

It is worth pointing out that CO oxidation shares some elementary steps with the water-gas shift (WGS) reaction [26,27]. The overall WGS reaction is $H_2O+CO \rightarrow H_2+CO_2$, where the oxidation of CO to CO_2 can occur as the direct process explained above ($CO+O_{\square}$), or through the COOH intermediate species, **Fig. 1**. CO conversion during WGS was shown to be much higher for ceria nanocubes compared to rod and octahedron nanoparticles [28], as also shown above for the CO oxidation

reaction. This comes either from an easier removal of the lattice oxygen by CO, or from an improved water activation due to the larger fraction of vacancies on the surface. Water can get activated at acid-base pair centers, such as Ce-O or □-O, and thus acidity and basicity control this step [131].

Table 4. Adsorption energies (in eV) of O_2, CO, CO_2, C_2H_2, and C_2H_4 on the clean and defective (111), (110), and (100) CeO_2 surfaces.

	(111)		(110)		(100)	
	clean	defective	clean	defective	clean	defective
O_2	-0.02	-1.86	-0.03	-1.03	-0.08	-2.22
CO	-0.20	-0.19	-0.24	-0.15	-0.34	-0.32
			-3.61 [a]		-4.34 [a]	-1.58
CO_2	-0.47 [a]	-0.99 [a]	-1.33 [a]	-0.93 [a]	-1.98 [a]	-2.65 [a]
C_2H_2	-0.08	-	-0.23	-	-0.27	-
	-0.30 [b]		-2.43 [c]		-4.05 [c]	
C_2H_4	-0.07	-	-0.22	-	-0.14	-
	0.28 [b]		-0.47 [c]		-2.76 [c]	

[a] Chemisorbed via carbonate formation. [b] Chemisorbed via O-[R]• radical formation.
[c] Chemisorbed via O-[R]-O formation.

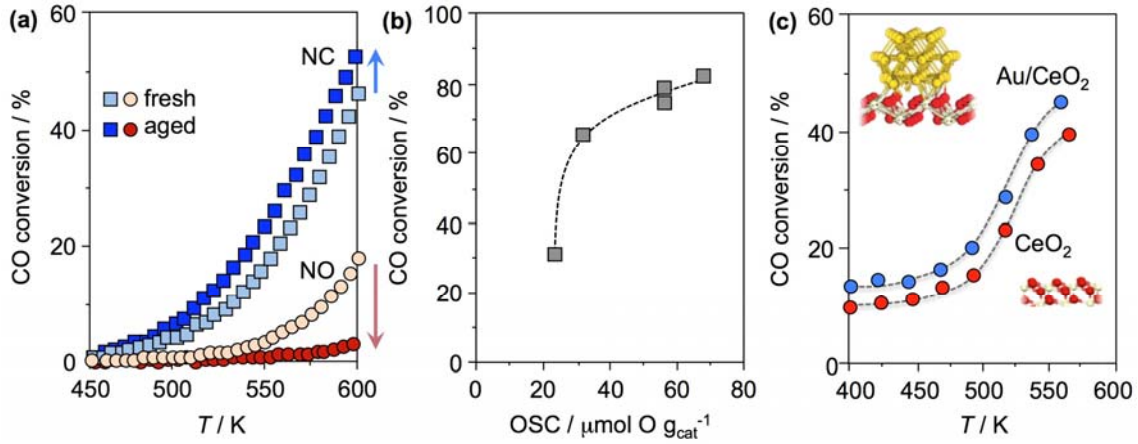

Fig. 6. (a) CO oxidation as a function of the temperature over ceria nanocubes (NC) and nanooctahedra (NO) fresh and aged. (b) CO oxidation as a function of the oxygen storage capacity in mixed $CeZrO_2$ oxides. (c) Performance of an Au/CeO_2 catalyst as a function of temperature. The model structure of the catalyst is shown in the inset. The figures are adapted from [112], [132], and [133], respectively.

3.2. Halogen production via hydrogen halide oxidation

A process for which ceria is close to industrial application is the recycling of chlorine by the gas-phase HCl oxidation [134,135]. Chlorine is employed to functionalize organic molecules and typically one atom gets included in the organic moiety. Furthermore, chlorine-containing compounds can be potentially hazardous and thus in many final products they need to be removed, usually in the form of HCl. The

oxidation of HCl to Cl_2 is an exothermic process carried out via a heterogeneous catalyst, typically RuO_2 [29,136–138]. However, RuO_2 is known to experience some stability issues at high temperatures [139]. On the other hand, CeO_2 possesses lower activity in the medium temperature regime, but its stability makes it a suitable candidate for the process in the reactor areas, where the temperature is known to raise [10]. The reaction network on CeO_2, **Fig. 7a**, was proposed to consist of the following steps:

$$HCl + O_{\square} + \square \rightarrow Cl_{\square} + O_{\square}H \quad (8)$$
$$HCl + O_{\square} + * \rightarrow Cl* + O_{\square}H \quad (9)$$
$$Cl_{\square} + Cl* \rightarrow Cl_2* + \square \quad (10)$$
$$Cl_2* \rightarrow Cl_2 + * \quad (11)$$
$$O_{\square}H + O_{\square}H \rightarrow H_2O_{\square} + O_{\square} \quad (12)$$
$$H_2O_{\square} \rightarrow H_2O + \square \quad (13)$$
$$O_2 + \square \rightarrow O_{2\square} \quad (14)$$
$$O_{2\square} + \square \rightarrow 2O_{\square} \quad (15)$$

HCl adsorbs dissociatively on ceria, where the halide fills a vacancy site leaving the system with a defect state as a Ce^{3+} atom. Further HCl adsorption then proceeds as Cl^- adsorbed on the surface. The first step relates to the acid-base and redox properties of the surface, whereas the latter only involves acid-base properties. Two Cl atoms from the surface and lattice positions can evolve toward the gas-phase, and the vacancy can be replenished by O_2. Therefore, the latter halide evolution and oxygen vacancy healing steps mainly involve redox properties, and also depend on the mobility of the vacancies in the material. Chlorine evolution is the most energy-demanding step, and thus the ability of the surface to rapidly cycle between Ce^{4+} and Ce^{3+} controls the activity. Therefore, the activity of ceria for HCl oxidation was shown to correlate with the experimental OSC measurements, **Fig. 7b**, performed on different CeO_2 samples.

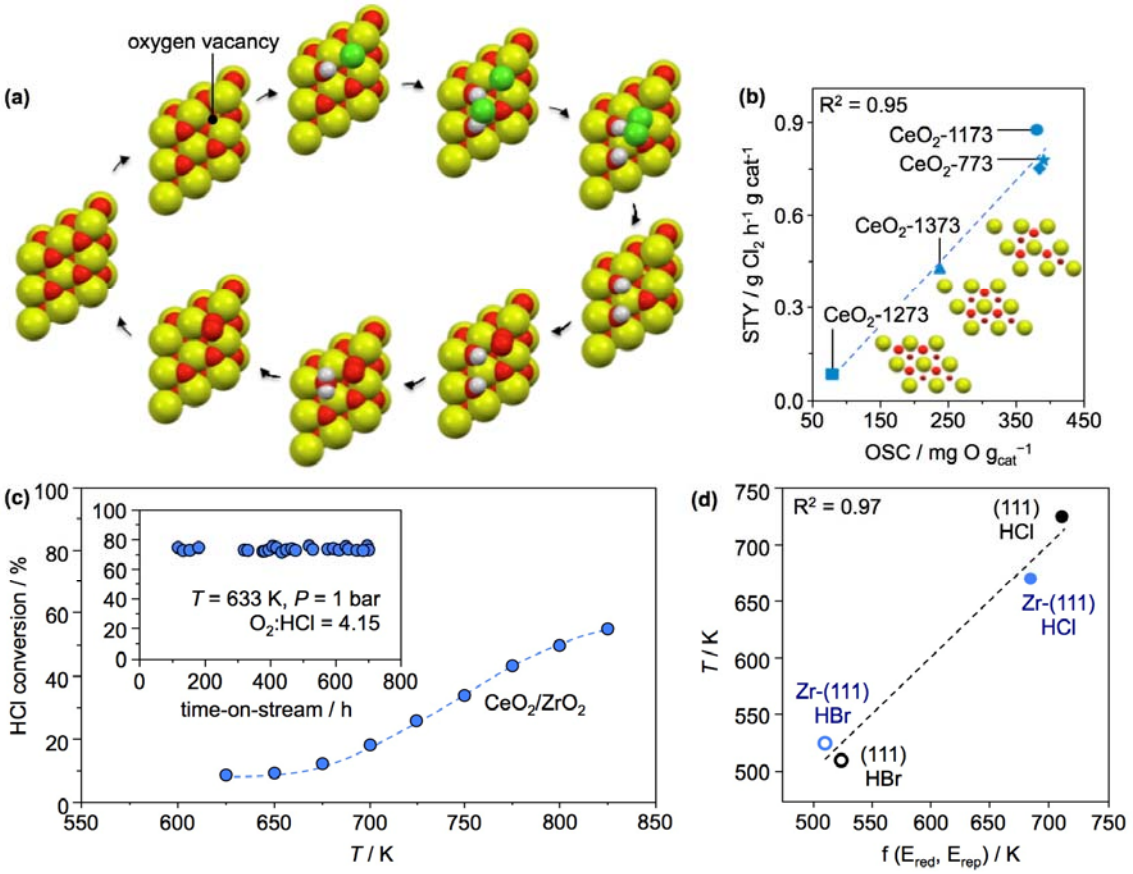

Fig. 7. (a) Mechanism of HCl oxidation over a CeO_2(111) surface. (b) Space-time yield as a function of the oxygen storage capacity of CeO_2. The temperatures indicate the temperature at which the oxide was calcined in static air, in order to alter the surface vacancy chemistry. (c) HCl conversion as a function of the temperature over CeO_2/ZrO_2 catalyst. The inset represents the stability of the catalyst for 800 h on stream. (d) Experimental light-off temperatures (at the rate of X_2 production, r = 3 mol X_2 mol Ce^{-1} h^{-1}) as a function of the two-variable descriptor involving E_{red} and E_{rep}, for Cl (filled dots) and Br (circles) on pristine (black) and Zr-doped (blue) ceria. The fitted equation is $f(E_{red}, E_{rep}) = (-522\ E_{red} + 777\ E_{rep} - 1)$ K. The figures (b) and (c) are adapted from [140] and [10].

Although the OSC character was shown to be the main activity descriptor, by the iso and aliovalent doping of ceria we found that the complexity of the reaction cannot be fully unveiled by this single parameter. While the activity increased for the isovalently doped ceria, trivalent dopant cations induced the opposite effect [31], which however cause a major enhance of the OSC behavior. The main responsible for this unintuitive behavior is that the redox character is better maintained through the isovalent doping, since trivalent cations generate $O^{\bullet}$ centers that are healed upon Cl adsorption, which ultimately annihilate the redox ability of the surface. The formation of these defect pairs can be characterized by the chlorine replacement energy, E_{rep}, of the lattice $CeO_2+1/2Cl_2 \rightarrow CeO_{2-x}Cl+1/2O_2$. For the pristine (111) surface, this E_{rep} is -0.40 eV, while it reaches -1.77 eV for the Ga-doped material. This means that the further step displacing the substituting chlorine (10) is a much higher energy-demanding

step for the latter doped material compared to the native surface. A similar conclusion was recently reached by Over and coworkers [33]. Remarkably, it is worth noting that the Zr-doped CeO_2 catalyst is not only more active than the pristine material, but also presents significantly high stability, **Fig. 7c** inset.

The chemistry found for HCl can be extended to heavier elements in the series, such as the recycling of HBr into Br_2 [32,141]. HBr oxidation always takes place at lower temperatures than HCl for all the studied materials, and the reaction is also more exothermic. The bigger radius of bromine compared to chlorine induces a decrease in the energy required to replace oxygen by the halide, E_{rep}, from -0.40 to -0.04 eV. These values turn more exothermic for the Zr-doped surface, -0.72 and -0.39 eV for Cl and Br, respectively. The lower stability of the Br-substituted surfaces makes HBr more active for the overall reaction. However, the redox character of the surface also plays a role, since the formation of X_2 (where X is Cl or Br) is a redox step (10). This is illustrated in **Fig. 7d**, where the light-off temperatures [32], at the X_2 production rate r = 3 mol X_2 mol Ce^{-1} h^{-1}, are shown to be a function of the two-variable descriptor embracing E_{rep} and E_{red}. Thus, both oxygen-halide replacement energy and surface redox ability need to be controlled to predict the light-off temperatures, for a given production rate.

3.3. Hydrogen activation and alkyne semi-hydrogenation

Excellent catalytic features of ceria have been also reported for hydrogenation reactions under hydrogen-rich conditions [35]. The key elementary step to understand this behavior is the activation of hydrogen, which is related to the presence of Ce-O short distances and charge separation [142–145]. Thus, H_2 is polarized and dissociates heterolytically on CeO_2 generating acid-base pairs on the surface (17) [146]. Alternatively, the homolytic dissociation over two surface oxygens is also possible (19), although it exhibits a slightly higher energy barrier [142]. The mechanisms are described as follows:

$$H_2 + * \rightarrow H_2* \quad (16)$$
$$H_2* + O_{\square} \rightarrow O_{\square}H + H* \quad (17)$$
$$H* + O_{\square} \rightarrow O_{\square}H + * \quad (18)$$
$$H_2* + 2O_{\square} \rightarrow 2O_{\square}H \quad (19)$$

The heterolytic mechanism results in a proton and a hydride attached to the basic and acid sites on the surface, thus acid (E_{CO}) and basic (O_{2p}) terms become relevant. The charge of the centers and their geometric distribution are crucial to understand the chemistry behind [142]. The reaction then proceeds, since the hydride can further move toward the equilibrium hydroxyl state (18), reducing two Ce surface centers. The latter step is thus associated to the reducibility of the surface, E_{red}. The final surface state is thus achieved via both the heterolytic and homolytic mechanisms. Therefore, the temperature of maximum H_2 consumption from the H_2-TPR on the three pristine surface

facets and the Ga-doped (111) correlates with the two-variable descriptor that includes the O_{2p} and E_{red} terms, **Fig. 8a**.

Hydrogen activation has been shown to be a key step in hydrogenation reactions [147]. Then, the hydrogenation mechanism has been reported to occur through two different pathways consisting of eq. (21) and (22-23):

$$C_2H_2 + * \rightarrow C_2H_2* \quad (20)$$
$$C_2H_2* + H_2* \rightarrow C_2H_4* + * \quad (21)$$
$$C_2H_2* + O_{\square}H \rightarrow C_2H_3* + O_{\square} \quad (22)$$
$$C_2H_3* + O_{\square}H \rightarrow C_2H_4* + O_{\square} \quad (23)$$
$$C_2H_4* \rightarrow C_2H_4 + * \quad (24)$$

The presence of large amounts of hydrogen in the environment leads to a majorly hydroxylated surface termination [147]. The reactivity is then controlled by the availability of sites on the substrate and the fact that H_2 activation is difficult. For the (111) surface, it was found that a concerted six-membered ring transition state in (21) comprising the alkyne C-C bond, the lattice OH, and the hydrogen molecule could be responsible for both the experimentally observed activity and selectivity [147]. An alternative mechanism was also proposed [148], where the alkyne adsorbs on the surface forming a radical species. This intermediate can strip the first hydrogen from the surface with a very low energy barrier (22), although the second H transfer (23) exhibits a large activation energy (>2.5 eV). Still some controversy on the nature of the reaction path exists, albeit recent NMR experiments seem to support the former mechanism [149]. Furthermore, if the reaction follows the concerted path, a stereoselectivity to the cis-alkene is expected over CeO_2. This is confirmed experimentally, showing full cis-alkene selectivity in the ceria-catalyzed hydrogenation of a variety of functionalized and internal acetylenic compounds [35].

The capability of the Ce-O pair to generate a large enough electric field that polarizes the incoming H_2 molecule is the most important point in the reactivity of the material in hydrogenations. This can be also traced back to the basicity of the surface and the redox term, together with the geometric ensemble that makes the transition state for hydrogen activation possible. This is likely to be extrapolated to the hydrogenation activity found for other oxides, such as ZrO_2 or La_2O_3 [150–152].

Face sensitivity of the reaction rate was also found in hydrogenation, where (111) facets show higher performance than the (100) exposing nanocubes [112]. The dependence was thus the opposite than that found for CO oxidation, **Fig. 8c**. Our description can explain this observation based on surface poisoning on the (100), **Table 4**. Strong adsorption is facilitated by basic centers on the surface and their adaptability to the coordination. On the (111) surface, alkynes adsorb on one basic center forming a radical intermediate with E_{ads} = -0.30 eV [148], whereas on the other surfaces the local structure allows coordination to two basic centers. Indeed, we have found an OCHCHO intermediate that sits on the surface in a robust manner, with coordination energy of -

4.05 and -2.41 on the (100) and (110) surfaces, respectively. This is reminiscent to carbonate poisoning in CO oxidation, and thus the basicity of the surface O_{2p} and the local coordination of the oxygens on the surface that allow their high mobility are the ultimate responsible for the observed poisoning.

The hydrogenation of alkynes is accelerated by the addition of trivalent dopants [36]. This has been experimentally shown in the gas-phase hydrogenation of alkynes over Ga-doped CeO_2 catalysts, **Fig. 8d**. It shall be noticed that for doped surfaces with trivalent cations the reaction mechanism is electronically different. The surface provides a localized hole state, located on the oxygen center near the doping atom, **Fig. 4**. Then the contribution from covalency becomes dominant and thus H_2 dissociation is homolytic. In the final state, the hole is filled with one of the electrons of the hydrogen molecule and the remaining $H^{\bullet}$ radical adsorbs on the adjacent cerium center. The ultimate consequence of this alternative mechanism is that the activation barrier for H_2 dissociation is much lower than for the regular surface. The best descriptor for the homolytic dissociation is then the energy of the hole on the surface, E_{red} (which in this particular case is related to the hole instead of the Ce^{4+}-Ce^{3+} cycle) [153,154]. In particular, trivalent cations were found to be more active in the following order: In > Ga > Al. The ordering closely follows the ionic radius of these dopants [36].

Other hydrogenation reactions over cerium oxide were also reported. Hydrogenation of benzoic acid to benzaldehyde, also under H_2 rich conditions, was performed exhibiting high activity and selectivity [151,155,156]. The reaction was suggested to proceed as a Mars-van-Krevelen mechanism, where the oxygen vacancy sites acted as the active sites. Hence, the (110) and (100) surfaces are more active than the (111). Likewise, the addition of dopants that increase the $E_{\square}$ and OSC promotes this reaction [151]. The hydrogenation of nitroaromatic compounds using N_2H_4 as a reducing agent was also performed on ceria nanoparticles, providing the related aniline derivative [157].

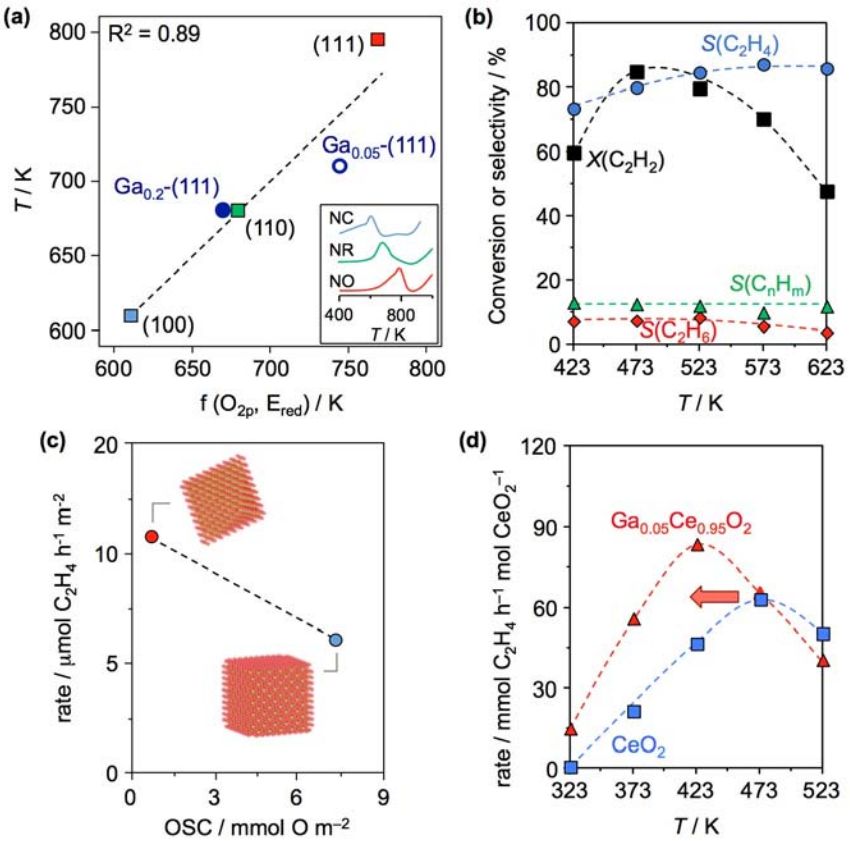

Fig. 8. (a) Temperature of maximum H_2 consumption during H_2-TPR as a function of the two-variable descriptor that includes the O_{2p} and E_{red} terms, for the (111), (110), (100), and $Ga_{0.2}Ce_{0.8}O_2$- and $Ga_{0.05}Ce_{0.95}O_2$-(111) surfaces. The fitted equation is $f(O_{2p}, E_{red}) = (426\ O_{2p} + 255\ E_{red} + 1001)$ K. The H_2 consumption TPR for nanoctahedra, nanorods, and nanocubes are shown in the inset. (b) Acetylene hydrogenation performance as a function of temperature over CeO_2. (c) Rate of acetylene hydrogenation as a function of the oxygen storage capacity over ceria nanoctahedra and nanocubes. (d) Influence of temperature on the activity of CeO_2 and $Ga_{0.05}Ce_{0.95}O_2$ in acetylene hydrogenation. The figure, in particular, depicts that Ga-doping enables a reduction of the operating temperature. Figures (b), (c), and (d) are adapted from [34], [112], and [36], respectively.

3.4. Alcohol conversion

Alcohol conversion has been extensively performed on ceria [37–46], since these reactive compounds are traditionally used as probe molecules to assess the catalytic properties of metal oxides [158,159]. Alcohols typically convert to aldehydes, following the proposed elementary steps listed below:

$$RCH_2OH + * \rightarrow RCH_2OH* \quad (25)$$
$$RCH_2OH* + O_{\square} \rightarrow RCH_2O* + O_{\square}H \quad (26)$$
$$RCH_2O* + O_{\square} \rightarrow RCHO* + O_{\square}H \quad (27)$$
$$RCHO* \rightarrow RCHO + * \quad (28)$$
$$O_{\square}H + O_{\square}H \rightarrow H_2O_{\square} + O_{\square} \quad (29)$$
$$H_2O_{\square} \rightarrow H_2O + \square \quad (30)$$

The first acid-base deprotonation step (26) precedes the redox C-H scission (27), where two cerium cations reduce to Ce^{3+}. For the acid-base step, the O_{2p} term controls the reaction rate, whereas the two-variable descriptor embracing O_{2p} and redox is required to describe the second step [108]. Oxygen vacancies however may play a role in this process, switching the selectivity to alkene formation through the following elementary steps:

$$RCH_2CH_2OH + \square + O_\square \rightarrow RCH_2CH_2O_\square + O_\square H \quad (31)$$
$$RCH_2CH_2O_\square + O_\square \rightarrow RCHCH_2O_\square + O_\square H \quad (32)$$
$$RCHCH_2O_\square + * \rightarrow RCH{=}CH_2* + O_\square \quad (33)$$
$$RCH{=}CH_2* \rightarrow RCH{=}CH_2 + * \quad (34)$$
$$O_\square H + O_\square H \rightarrow H_2O_\square + O_\square \quad (35)$$
$$H_2O_\square \rightarrow H_2O + \square \quad (36)$$

Thus, in addition to the O_{2p} and E_{red} terms to describe the O-H (31) and C-H (32) scissions, the oxygen vacancy formation energy determines the rate of this side reaction and thus the overall selectivity.

As demonstrated experimentally, alcohol conversion is also structure sensitive [39,40,42]. The rate of methanol and ethanol conversion is higher on the (100) surface than on the (111) surface. This is attributed to the fact that the activation energy for C-H cleavage is much lower on the (100) surface, due to its higher redox ability. Furthermore, for the conversion of ethanol, a temperature increase favors the formation of ethylene over acetaldehyde on the (100) compared to the (111) facet [42]. This is due to the lower oxygen vacancy formation energy for the former surface (**Table 2**).

For the particular case of methanol, the subsequent oxidation of formaldehyde to CO was also observed in the more open (100) surface. The reaction consists of the following elementary steps:

$$HCHO* + O_\square \rightarrow CHO* + O_\square H \quad (37)$$
$$CHO* + O_\square \rightarrow CO* + O_\square H \quad (38)$$
$$CO* \rightarrow CO + * \quad (39)$$
$$O_\square H + O_\square H \rightarrow H_2O_\square + O_\square \quad (40)$$
$$H_2O_\square \rightarrow H_2O + \square \quad (41)$$

Therefore the competition between formaldehyde desorption and the first C-H cleavage of formaldehyde triggers the selectivity [160]. The first step of this reaction is a redox step, where formaldehyde is oxidized and surface is reduced. The second C-H scission is an acid-base step. To describe the first C-H stripping, O_{2p} and E_{red} terms are crucial, analogous to the C-H bond breaking in methanol. **Fig. 9** shows the correlation of the activation energy of this elementary step with respect to the combined O_{2p} and

E_{red} terms, for the three low-index surfaces and the isovalent and aliovalent doped-(111). Both the basicity of the recipient oxygen and the capability of the surface to accommodate the two electrons formaldehyde oxidation are required to describe this step. For the second H-stripping, only the O_{2p} is required as it is an acid-base step. In addition, to assess the selectivity, formaldehyde desorption must be also described. Formaldehyde chemisorbs on ceria as a bidentate structure forming Ce-O and $O_{\square}$-C bonds. Then the acidity of the cerium cations, the basicity of the oxygens, and the site structure control how the bidentate adsorbate accommodates on the surface [108].

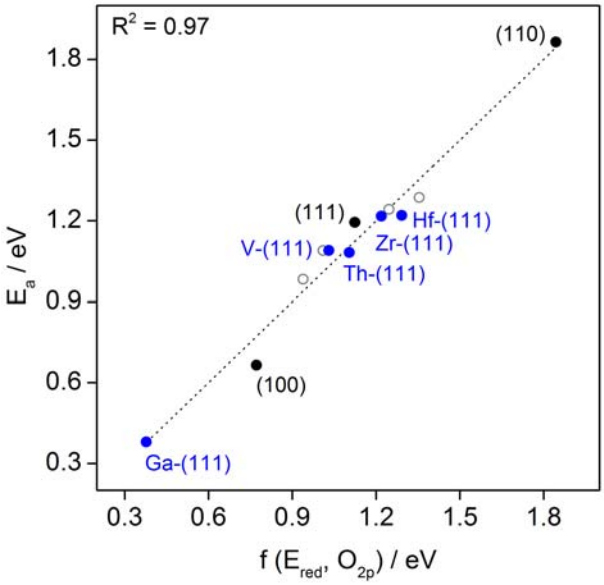

Fig. 9. Formaldehyde first C-H scission activation energy as a function of a collective variable embracing E_{red} and O_{2p}, for the pristine (111), (110, and (100) CeO_2 surfaces and the doped Ga-, V-, Zr-, Hf-, and Th-(111) surfaces. The implicit doped (111) structures obtained from applying strain to the (111) surface are also included (grey circles). The fitted equation is $f(E_{red}, O_{2p}) = (0.57\ E_{red} - 0.83\ O_{2p} + 0.02)$ eV. The Hf-, Th-, and strained (111) values are adapted from [108].

The (100) surface has higher cerium acidity, oxygen basicity, and larger site area than the (111) or the (110) surfaces, and thus HCHO binds stronger on this facet. Furthermore, the high inherent number of vacancy sites on the (100) facet also favors the adsorption of O-R compounds. Similarly, the higher redox ability of the (100) surface in combination with the oxygen basicity favors C-H scission on this facet. Formaldehyde hence converts to CO on the (100) surface, whereas it desorbs from the (111) and (110) surfaces, as observed in the TPD experiments and the DFT energy profiles [39,160].

3.5. Dimethyl carbonate synthesis via CO_2 valorization

More sophisticated reactions to valorize CO_2 [44,52,161–164] have been recently put forward. For example, CO_2 from waste effluents can react with methanol to

form dimethyl carbonate (DMC), an important intermediate for polycarbonates and fuel additives. CeO_2 catalysts have been proposed as suitable active materials for this family of reactions. The overall reaction is as follows:

$$CO_2 + 2MeOH \rightleftarrows CH_3OCOOCH_3 + H_2O \quad (42)$$

The equilibrium of the reaction is driven toward reactants unless water is removed from the medium employing a sorbent. The proof-of-principle of the higher conversion when employing a dehydrating agent was presented by Tomishige and coworkers [53,54], and recently a continuous process employing relatively high pressures for the CO_2 has been developed [55].

The list of elementary reactions potentially participating in the process is as follows:

$$CO_2 + * \rightarrow CO_2* \quad (43)$$
$$CH_3OH + * \rightarrow CH_3OH* \quad (44)$$
$$CH_3OH* + O_{\square} \rightarrow CH_3O* + O_{\square}H \quad (45)$$
$$CO_2* + CH_3O* \rightarrow CO_2OCH_3* + * \quad (46)$$
$$CO_2OCH_3* + O_{\square}H \rightarrow HOCOOCH_3* + O_{\square} \quad (47)$$
$$HOCOOCH_3* + CH_3O* \rightarrow CH_3OCOOCH_3* + OH* \quad (48)$$
$$OH* + O_{\square}H \rightarrow H_2O* + O_{\square} \quad (49)$$
$$CH_3OCOOCH_3* \rightarrow CH_3OCOOCH_3 + * \quad (50)$$
$$H_2O* \rightarrow H_2O + * \quad (51)$$

The adsorption of CO_2 depends on the basicity of the surface, O_{2p}, in agreement with our previous results and experimentally illustrated by Jung et al. [70]. As we have shown earlier, methanol adsorption (44) precedes an acid-base dissociation (45). On the clean surface the Ce-O pairs act as such centers. It shall be noticed that the basicity of O_{2p} is involved in both CO_2 trapping and CH_3OH adsorption. As methanol reacts easily with the surface, the need of high CO_2 pressure can be explained as the competition for the adsorption on the basic sites of the surface. The subsequent reaction steps can be understood as a substitution where CO_2 is attacked by the methoxy group. At this stage, the carbonate gets protonated to improve its ability as leaving group. The ligand displacement by another methoxy group on the surface would generate a surface hydroxyl group and the DMC, weakly bound to the surface. The recombination of OH with another proton from the surface leads to the secondary water product.

The mechanistic analysis indicates that the following descriptors are crucial for DMC synthesis. First, both the basicity and the acidity of the material are required to initiate the reaction. However, a high acidity of the material has been described as detrimental to the overall performance. The reason for that can be traced back to the fact that steps (46) and (47) are limited by the presence of strong acid (Brønsted) sites as clean basic O centers are needed on the surface. Still, some degree of acidity is needed to eliminate water from the surface (51). This explains the acid-base promotion found

experimentally [70]. Moreover, the mechanism sketched above provides two major threats. On the one hand, areas with high density of vacancies where some of the carbonates can be trapped will activate the internal bonds in undesired manners. Therefore, facets or doping that improve the formation of vacancies or contain more vacancies would be less efficient to form DMC. An alternative way of illustrating this is by inferring the size required for the reaction ensemble. While the reactions described before dimethyl carbonate synthesis required only a very few adsorption sites, the large hapticity of the fragments involved in this reaction implies that the isolation of sites is not a good strategy in DMC synthesis.

4. Conclusions and outlook

The applications of CeO_2 in heterogeneous catalysis have expanded over the last years. The flexibility of the electronic structure able to be reduced, the acid-base properties of the surface, and its resistance against harsh reactions conditions make it suitable for many uses. These versatile and unique catalytic properties turn ceria an optimal playground to make a real step forward in catalysis. In this perspective, the synergy between careful synthetic shape control at the nanoscale, accurate characterization, catalytic testing, and extensive use of the computational techniques for the rationalization and prediction of the properties are gathered and described. The oxygen activation properties have been taken as the main characteristics of the material, thus being mainly employed in traditional oxidation processes like CO and soot. However, these properties have been extended to other challenging oxidation processes, like those of hydrogen halides (HCl and HBr) for halogen recovery. Complementary reactions including alkyne semi-hydrogenation have been also reported recently and are being extended to other oxides. Other reactions that are basically centered in the reduction of methanol to formaldehyde and the condensation of methanol with CO_2 to dimethylcarbonate have also been proposed. This wide variety of reactions can be systematized based on descriptors for the reactivity. Starting from the classical terms described by Grasselli, which are non-ortogonal, we have developed a full set of chemical descriptors that can be used to describe the reactivity of these materials and that can be either experimentally or computationally derived. In most cases, due to some difficulties in either shape-selected synthesis or precise characterization, it is easier to calculate these descriptors from first-principles. Our results show that it is possible to trace back the reactivity and stability of materials mainly through the introduction of basicity, redox, and geometric terms.

The present results thus present a systematic way of how catalysis by ceria and doped-ceria materials can be analyzed. We consider that this is the first step towards the prediction of more active and selective surfaces (or doped systems) for the next generation of ceria-based materials. Improving the performance via chemical descriptors is a much more intuitive approach than other structure-activity relationships based on energies, as they are directly meaningful and might be benchmarked against

experimental descriptors. Finally, the approach provided herein to describe the catalysis of ceria can be extended to other families of complex compounds including oxides, carbides, sulphides, and multicomponent materials with acid-base and/or redox sites, and employed to oxidations, reductions, acid-base, and associative reactions. The procedure then shall enclose: (i) determination of the phases under reaction conditions; (ii) experimental and first-principles thermodynamics to analyze the state of the surface (stoichiometry, geometry, etc); and finally, (iii) reduce the complete set of chemical descriptors to the meaningful ones for a particular reaction, experimental conditions, and/or material.

Acknowledgements

N.L. acknowledges the Ministerio de Economía y Competitividad – MINECO (CTQ2012-33826), and the Generalitat de Catalunya – AGAUR (SGR-2014-SGR-145), as well as the BSC-RES for providing generous computational resources. M.C.-C. is grateful to MINECO for a "Juan de la Cierva – Formación" fellowship (FJCI-2014-20568). J.P.-R. thanks the Swiss National Science Foundation (project no. 2-77204-14).

Appendix A. Supplementary material

Supplementary data associated with this article can be found, in the online version.

References

[1] A. Trovarelli, Catalysis by Ceria and Related Materials, Imperial College Press, London, 2002.

[2] W. Huang, Y. Gao, Catal. Sci. Technol. 4 (2014) 3772–3784.

[3] C. Sun, H. Li, L. Chen, Energy Environ. Sci. 5 (2012) 8475.

[4] D. Zhang, X. Du, L. Shi, R. Gao, Dalton Trans. 41 (2012) 14455–75.

[5] Z.-A. Qiao, Z. Wu, S. Dai, ChemSusChem. 6 (2013) 1821–33.

[6] H. Metiu, S. Chrétien, Z. Hu, B. Li, X. Sun, J. Phys. Chem. C. 116 (2012) 10439–10450.

[7] A. Trovarelli, Catal. Rev. 38 (1996) 439–520.

[8] M.V. Ganduglia-Pirovano, A. Hofmann, J. Sauer, Surf. Sci. Rep. 62 (2007) 219–270.

[9] J. Paier, C. Penschke, J. Sauer, Chem. Rev. 113 (2013) 3949–85.

[10] A.P. Amrute, C. Mondelli, M. Moser, G. Novell-Leruth, N. López, D. Rosenthal, et al., J. Catal. 286 (2012) 287–297.

[11] D.A. Andersson, S.I. Simak, N. V Skorodumova, I.A. Abrikosov, B. Johansson, Proc. Natl. Acad. Sci. U. S. A. 103 (2006) 3518–21.

[12] J.S. Elias, M. Risch, L. Giordano, A.N. Mansour, Y. Shao-Horn, J. Am. Chem. Soc. 136 (2014) 17193–200.

[13] G. Azimi, R. Dhiman, H.-M. Kwon, A.T. Paxson, K.K. Varanasi, Nat. Mater. 12 (2013) 315–20.

[14] G. Carchini, M. García-Melchor, Z. Łodziana, N. López, ACS Appl. Mater. Interfaces. 8 (2016) 152–60.

[15] F. Esch, S. Fabris, L. Zhou, T. Montini, C. Africh, P. Fornasiero, et al., Science. 309 (2005) 752–5.

[16] M. Nolan, S.C. Parker, G.W. Watson, Surf. Sci. 595 (2005) 223–232.

[17] D.R. Mullins, Surf. Sci. Rep. 70 (2015) 42–85.

[18] C.T. Campbell, C.H.F. Peden, Science. 309 (2005) 713–4.

[19] H.C. Yao, Y.F.Y. Yao, J. Catal. 86 (1984) 254–265.

[20] E.P. Murray, T. Tsai, S.A. Barnett, 400 (1999) 649–651.

[21] S. Park, J. Vohs, R. Gorte, Nature. 404 (2000) 265–7.

[22] B.C. Steele, A. Heinzel, Nature. 414 (2001) 345–52.

[23] Z. Shao, S.M. Haile, Nature. 431 (2004) 170–3.

[24] M.M. Schubert, V. Plzak, J. Garche, R.J. Behm, Catal. Letters. 76 (2001) 143–150.

[25] O. Pozdnyakova, D. Teschner, A. Wootsch, J. Kröhnert, B. Steinhauer, H. Sauer, et al., J. Catal. 237 (2006) 1–16.

[26] J.B. Park, J. Graciani, J. Evans, D. Stacchiola, S. Ma, P. Liu, et al., Proc. Natl. Acad. Sci. U. S. A. 106 (2009) 4975–80.

[27] J.A. Rodriguez, S. Ma, P. Liu, J. Hrbek, J. Evans, M. Pérez, Science. 318 (2007) 1757–60.

[28] S. Agarwal, L. Lefferts, B.L. Mojet, D.A.J.M. Ligthart, E.J.M. Hensen, D.R.G. Mitchell, et al., ChemSusChem. 6 (2013) 1898–906.

[29] J. Pérez-Ramírez, C. Mondelli, T. Schmidt, O.F.-K. Schlüter, A. Wolf, L. Mleczko, et al., Energy Environ. Sci. 4 (2011) 4786–4799.

[30] R. Farra, M. Eichelbaum, R. Schlögl, L. Szentmiklósi, T. Schmidt, A.P. Amrute, et al., J. Catal. 297 (2013) 119–127.

[31] R. Farra, M. García-Melchor, M. Eichelbaum, M. Hashagen, W. Frandsen, J. Allan, et al., ACS Catal. 3 (2013) 2256–2268.

[32] M. Moser, G. Vilé, S. Colussi, F. Krumeich, D. Teschner, L. Szentmiklósi, et al., J. Catal. 331 (2015) 128–137.

[33] M. Möller, S. Urban, P. Cop, T. Weller, R. Ellinghaus, M. Kleine-Boymann, et al., ChemCatChem (2015) DOI: 10.1002/cctc.201500712.

[34] G. Vilé, B. Bridier, J. Wichert, J. Pérez-Ramírez, Angew. Chem. Int. Ed. 51 (2012) 8620–3.

[35] G. Vilé, S. Wrabetz, L. Floryan, M.E. Schuster, F. Girgsdies, D. Teschner, et al., ChemCatChem. 6 (2014) 1928–1934.

[36] G. Vilé, P. Dähler, J. Vecchietti, M. Baltanás, S. Collins, M. Calatayud, et al., J. Catal. 324 (2015) 69–78.

[37] R.M. Ferrizz, G.S. Wong, T. Egami, J.M. Vohs, Langmuir. 17 (2001) 2464–2470.

[38] D.R. Mullins, M.D. Robbins, J. Zhou, Surf. Sci. 600 (2006) 1547–1558.

[39] P.M. Albrecht, D.R. Mullins, Langmuir. 29 (2013) 4559–67.

[40] Z. Wu, M. Li, D.R. Mullins, S.H. Overbury, ACS Catal. 2 (2012) 2224–2234.

[41] V. Matolín, J. Libra, M. Škoda, N. Tsud, K.C. Prince, T. Skála, Surf. Sci. 603 (2009) 1087–1092.

[42] M. Li, Z. Wu, S.H. Overbury, J. Catal. 306 (2013) 164–176.

[43] Y. Lykhach, A. Neitzel, K. Ševčíková, V. Johánek, N. Tsud, T. Skála, et al., ChemSusChem. 7 (2014) 77–81.

[44] M.H. Haider, N.F. Dummer, D.W. Knight, R.L. Jenkins, M. Howard, J. Moulijn, et al., Nat. Chem. (2015) DOI: 10.1038/nchem.2345.

[45] D.R. Mullins, S.D. Senanayake, T.-L. Chen, J. Phys. Chem. C. 114 (2010) 17112–17119.

[46] T.-L. Chen, D.R. Mullins, J. Phys. Chem. C. 115 (2011) 13725–13733.

[47] T.-L. Chen, D.R. Mullins, J. Phys. Chem. C. 115 (2011) 3385–3392.

[48] F.C. Calaza, Y. Xu, D.R. Mullins, S.H. Overbury, J. Am. Chem. Soc. 134 (2012) 18034–45.

[49] A.K.P. Mann, Z. Wu, F.C. Calaza, S.H. Overbury, ACS Catal. 4 (2014) 2437–2448.

[50] S.M. Schimming, O.D. LaMont, M. König, A.K. Rogers, A.D. D'Amico, M.M. Yung, et al., ChemSusChem. 8 (2015) 2073–83.

[51] S.D. Senanayake, W.O. Gordon, S.H. Overbury, D.R. Mullins, J. Phys. Chem. C. 113 (2009) 6208–6214.

[52] M. Honda, M. Tamura, Y. Nakagawa, S. Sonehara, K. Suzuki, K.-I. Fujimoto, et al., ChemSusChem. 6 (2013) 1341–4.

[53] K. Tomishige, Y. Furusawa, Y. Ikeda, M. Asadullah, K. Fujimoto, Catal. Letters. 76 (2001) 71–74.

[54] K. Tomishige, K. Kunimori, Appl. Catal. A Gen. 237 (2002) 103–109.

[55] A. Bansode, A. Urakawa, ACS Catal. 4 (2014) 3877–3880.

[56] J.A. Rodriguez, T. Jirsak, S. Sambasivan, D. Fischer, A. Maiti, J. Chem. Phys. 112 (2000) 9929.

[57] R.M. Ferrizz, T. Egami, G.S. Wong, J.M. Vohs, Surf. Sci. 476 (2001) 9–21.

[58] M. Daturi, N. Bion, J. Saussey, J.-C. Lavalley, C. Hedouin, T. Seguelong, et al., Phys. Chem. Chem. Phys. 3 (2001) 252–255.

[59] M. Waqif, P. Bazin, O. Saur, J.C. Lavalley, G. Blanchard, O. Touret, Appl. Catal. B Environ. 11 (1997) 193–205.

[60] J.A. Rodriguez, T. Jirsak, A. Freitag, J.C. Hanson, J.Z. Larese, S. Chaturvedi, Catal. Letters. 62 (1999) 113–119.

[61] S.H. Overbury, D.R. Mullins, D.R. Huntley, L. Kundakovic, J. Phys. Chem. B. 103 (1999) 11308–11317.

[62] R.M. Ferrizz, R.J. Gorte, J.M. Vohs, Catal. Letters. 82 (2002) 123–129.

[63] M.Y. Smirnov, A. V Kalinkin, A. V Pashis, A.M. Sorokin, A.S. Noskov, K.C. Kharas, et al., J. Phys. Chem. B. 109 (2005) 11712–9.

[64] M. Happel, Y. Lykhach, N. Tsud, T. Skála, K.C. Prince, V. Matolín, et al., J. Phys.

Chem. C. 115 (2011) 19872–19882.

[65] M. Flytzani-Stephanopoulos, M. Sakbodin, Z. Wang, Science. 312 (2006) 1508–10.

[66] D.R. Mullins, T.S. McDonald, Surf. Sci. 601 (2007) 4931–4938.

[67] B. Liu, H. Xu, Z. Zhang, Chinese J. Catal. 33 (2012) 1631–1635.

[68] C. Binet, M. Daturi, J.-C. Lavalley, Catal. Today. 50 (1999) 207–225.

[69] Z. Wu, M. Li, S.H. Overbury, J. Catal. 285 (2012) 61–73.

[70] H.J. Lee, S. Park, I.K. Song, J.C. Jung, Catal. Letters. 141 (2011) 531–537.

[71] Z. Wu, A.K.P. Mann, M. Li, S.H. Overbury, J. Phys. Chem. C. 119 (2015) 7340–7350.

[72] M. Boronat, T. López-Ausens, A. Corma, Surf. Sci. (2015) DOI: 10.1016/j.susc.2015.10.047.

[73] L. Vivier, D. Duprez, ChemSusChem. 3 (2010) 654–78.

[74] J.K. Nørskov, T. Bligaard, B. Hvolbæk, F. Abild-Pedersen, I. Chorkendorff, C.H. Christensen, Chem. Soc. Rev. 37 (2008) 2163–2171.

[75] F. Studt, F. Abild-Pedersen, T. Bligaard, R.Z. Sørensen, C.H. Christensen, J.K. Nørskov, Science. 320 (2008) 1320–2.

[76] F. Calle-Vallejo, D. Loffreda, M.T.M. Koper, P. Sautet, Nat. Chem. 7 (2015) 403–410.

[77] P. Sabatier, La catalyse en chimie organique, Librairie Polytechnique, Paris, 1920.

[78] R.K. Grasselli, Top. Catal. 21 (2002) 79–88.

[79] W. Tang, E. Sanville, G. Henkelman, J. Phys. Condens. Matter. 21 (2009) 084204.

[80] P.A. Redhead, Vacuum. 12 (1962) 203–211.

[81] Although many clear probes for basic/acid sites are commonly available, polar reactants may dissociate upon interaction with the surface (e.g. acid molecules), making impossible to disentangle the contributions.

[82] Care shall be taken though as probably the number of potential acceptors (i.e. in high symmetry positions) that can stabilize by polarons is relevant to the overall redox ability.

[83] The electron added was localized on one single Ce(III) cation. Charge compensation is applied on these non-neutral unit cells by the addition of a homogeneous background charge. This is sensitive to the vacuum width, which must be kept constant on the different calculations.

[84] C. Sachs, M. Hildebrand, S. Volkening, J. Wintterlin, G. Ertl, Science. 293 (2001) 1635–8.

[85] C. Sachs, M. Hildebrand, S. Völkening, J. Wintterlin, G. Ertl, J. Chem. Phys. 116 (2002) 5759.

[86] K. Reuter, M. Scheffler, Phys. Rev. Lett. 90 (2003) 046103.

[87] D. Teschner, G. Novell-Leruth, R. Farra, A. Knop-Gericke, R. Schlögl, L. Szentmiklósi, et al., Nat. Chem. 4 (2012) 739–45.

[88] J. Carrasco, N. Lopez, F. Illas, Phys. Rev. Lett. 93 (2004) 225502.

[89] M. Ganduglia-Pirovano, J. Da Silva, J. Sauer, Phys. Rev. Lett. 102 (2009) 026101.

[90] X. Wang, A. Chaka, M. Scheffler, Phys. Rev. Lett. 84 (2000) 3650–3.

[91] M. V. Bollinger, K.W. Jacobsen, J.K. Nørskov, Phys. Rev. B. 67 (2003) 085410.

[92] Z.-G. Yan, C.-H. Yan, J. Mater. Chem. 18 (2008) 5046.

[93] C. Noguera, J. Phys. Condens. Matter. 12 (2000) R367–R410.

[94] G.S. Herman, Phys. Rev. B. 59 (1999) 14899–14902.

[95] Y.J. Kim, Y. Gao, G.S. Herman, S. Thevuthasan, W. Jiang, D.E. McCready, et al., J. Vac. Sci. Technol. A Vacuum, Surfaces, Film. 17 (1999) 926.

[96] H. Nörenberg, J.H. Harding, Surf. Sci. 477 (2001) 17–24.

[97] M. Nolan, S. Grigoleit, D.C. Sayle, S.C. Parker, G.W. Watson, Surf. Sci. 576 (2005) 217–229.

[98] P.M. Albrecht, D. Jiang, D.R. Mullins, J. Phys. Chem. C. 118 (2014) 9042–9050.

[99] P. Geysermans, F. Finocchi, J. Goniakowski, R. Hacquart, J. Jupille, Phys. Chem. Chem. Phys. 11 (2009) 2228–33.

[100] J. V Lauritsen, S. Porsgaard, M.K. Rasmussen, M.C.R. Jensen, R. Bechstein, K. Meinander, et al., ACS Nano. 5 (2011) 5987–94.

[101] D.O. Scanlon, N.M. Galea, B.J. Morgan, G.W. Watson, J. Phys. Chem. C. 113 (2009) 11095–11103.

[102] M. Nolan, Chem. Phys. Lett. 499 (2010) 126–130.

[103] J. Goniakowski, F. Finocchi, C. Noguera, Reports Prog. Phys. 71 (2008) 016501.

[104] P. Oliver, G. Watson, S. Parker, Phys. Rev. B. 52 (1995) 5323–5329.

[105] M. Salciccioli, Y. Chen, D.G. Vlachos, J. Phys. Chem. C. 114 (2010) 20155–20166.

[106] M. Salciccioli, S.M. Edie, D.G. Vlachos, J. Phys. Chem. C. 116 (2012) 1873–1886.

[107] R. García-Muelas, N. López, J. Phys. Chem. C. 118 (2014) 17531–17537.

[108] M. Capdevila-Cortada, N. López, ACS Catal. (2015) 6473–6480.

[109] H.-X. Mai, L.-D. Sun, Y.-W. Zhang, R. Si, W. Feng, H.-P. Zhang, et al., J. Phys. Chem. B. 109 (2005) 24380–5.

[110] E. Aneggi, D. Wiater, C. de Leitenburg, J. Llorca, A. Trovarelli, ACS Catal. 4 (2014) 172–181.

[111] E. Aneggi, J. Llorca, M. Boaro, A. Trovarelli, J. Catal. 234 (2005) 88–95.

[112] G. Vilé, S. Colussi, F. Krumeich, A. Trovarelli, J. Pérez-Ramírez, Angew. Chem. Int. Ed. 53 (2014) 12069–72.

[113] M. Nolan, G.W. Watson, J. Phys. Chem. B. 110 (2006) 16600–6.

[114] M. Nolan, S.C. Parker, G.W. Watson, Surf. Sci. 600 (2006) 175–178.

[115] R. Farra, S. Wrabetz, M.E. Schuster, E. Stotz, N.G. Hamilton, A.P. Amrute, et al., Phys. Chem. Chem. Phys. 15 (2013) 3454–3465.

[116] M. Huang, S. Fabris, Phys. Rev. B. 75 (2007) 081404.

[117] H.-T. Chen, J.-G. Chang, H.-L. Chen, S.-P. Ju, J. Comput. Chem. 30 (2009) 2433–42.

[118] Z. Wu, M. Li, J. Howe, H.M. Meyer, S.H. Overbury, Langmuir. 26 (2010) 16595–606.

[119] O.H. Laguna, A. Pérez, M.A. Centeno, J.A. Odriozola, Appl. Catal. B Environ. 176-177 (2015) 385–395.

[120] T. Vinodkumar, B.G. Rao, B.M. Reddy, Catal. Today. 253 (2015) 57–64.

[121] Q. Fu, H. Saltsburg, M. Flytzani-Stephanopoulos, Science. 301 (2003) 935–8.

[122] R. Si, M. Flytzani-Stephanopoulos, Angew. Chem. Int. Ed. 47 (2008) 2884–7.

[123] Z. Zhou, S. Kooi, M. Flytzani-Stephanopoulos, H. Saltsburg, Adv. Funct. Mater. 18 (2008) 2801–2807.

[124] J.A. Rodriguez, P. Liu, J. Hrbek, J. Evans, M. Pérez, Angew. Chem. Int. Ed. 46 (2007) 1329–32.

[125] H.Y. Kim, G. Henkelman, J. Phys. Chem. Lett. 4 (2013) 216–21.

[126] M. Fernández-García, A. Martínez-Arias, L.N. Salamanca, J.M. Coronado, J.A. Anderson, J.C. Conesa, et al., J. Catal. 187 (1999) 474–485.

[127] S. Hinokuma, H. Fujii, M. Okamoto, K. Ikeue, M. Machida, Chem. Mater. 22 (2010) 6183–6190.

[128] M. Kurnatowska, L. Kepinski, W. Mista, Appl. Catal. B Environ. 117 (2012) 135–147.

[129] R.V. Gulyaev, E.M. Slavinskaya, S.A. Novopashin, D.V. Smovzh, A.V. Zaikovskii, D.Y. Osadchii, et al., Appl. Catal. B Environ. 147 (2014) 132–143.

[130] G.N. Vayssilov, Y. Lykhach, A. Migani, T. Staudt, G.P. Petrova, N. Tsud, et al., Nat. Mater. 10 (2011) 310–5.

[131] D. Fernández-Torre, K. Kośmider, J. Carrasco, M.V. Ganduglia-Pirovano, R. Pérez, J. Phys. Chem. C. 116 (2012) 13584–13593.

[132] M. Boaro, C. de Leitenburg, G. Dolcetti, A. Trovarelli, J. Catal. 193 (2000) 338–347.

[133] J. Qi, J. Chen, G. Li, S. Li, Y. Gao, Z. Tang, Energy Environ. Sci. 5 (2012) 8937.

[134] T. Schmidt, A. Wolf, O.F.-K. Sch, T. Westermann, C. Mondelli, J. Perez-Ramirez, et al., WO2013004651, 2013.

[135] T. Schmidt, A. Wolf, O.F.-K. Schluter, T. Westermann, C. Mondelli, J. Perez-Ramirez, et al., WO2013004649, 2013.

[136] N. López, J. Gómez-Segura, R.P. Marín, J. Pérez-Ramírez, J. Catal. 255 (2008) 29–39.

[137] D. Crihan, M. Knapp, S. Zweidinger, E. Lundgren, C.J. Weststrate, J.N. Andersen, et al., Angew. Chem. Int. Ed. 47 (2008) 2131–4.

[138] H. Over, J. Phys. Chem. C. 116 (2012) 6779–6792.

[139] H. Over, Chem. Rev. 112 (2012) 3356–426.

[140] M. Moser, C. Mondelli, T. Schmidt, F. Girgsdies, M.E. Schuster, R. Farra, et al., Appl. Catal. B Environ. 132-133 (2013) 123–131.

[141] M. Moser, I. Czekaj, N. López, J. Pérez-Ramírez, Angew. Chem. Int. Ed. 53 (2014) 8628–33.

[142] M. García-Melchor, N. López, J. Phys. Chem. C. 118 (2014) 10921–10926.

[143] D. Fernández-Torre, J. Carrasco, M.V. Ganduglia-Pirovano, R. Pérez, J. Chem. Phys. 141 (2014) 014703.

[144] F.R. Negreiros, M.F. Camellone, S. Fabris, J. Phys. Chem. C. 119 (2015) 21567–21573.

[145] J. Höcker, T.O. Menteş, A. Sala, A. Locatelli, T. Schmidt, J. Falta, et al., Adv. Mater. Interfaces (2015) DOI: 10.1002/admi.201500314.

[146] Z. Hu, H. Metiu, J. Phys. Chem. C. 116 (2012) 6664–6671.

[147] M. García-Melchor, L. Bellarosa, N. López, ACS Catal. 4 (2014) 4015–4020.

[148] J. Carrasco, G. Vilé, D. Fernández-Torre, R. Pérez, J. Pérez-Ramírez, M.V. Ganduglia-Pirovano, J. Phys. Chem. C. 118 (2014) 5352–5360.

[149] E.W. Zhao, H. Zheng, R. Zhou, H.E. Hagelin-Weaver, C.R. Bowers, Angew. Chem. Int. Ed. (2015) DOI: 10.1002/anie.201506045.

[150] E.J. Grootendorst, R. Pestman, R.M. Koster, V. Ponec, J. Catal. 148 (1994) 261–269.

[151] Y. Sakata, V. Ponec, Appl. Catal. A Gen. 166 (1998) 173–184.

[152] S. Chrétien, H. Metiu, J. Phys. Chem. C. 119 (2015) 19876–19882.

[153] N. López, C. Vargas-Fuentes, Chem. Commun. 48 (2012) 1379–91.

[154] G. Novell-Leruth, G. Carchini, N. López, J. Chem. Phys. 138 (2013) 194706.

[155] T. Yokoyama, N. Yamagata, Appl. Catal. A Gen. 221 (2001) 227–239.

[156] M. Chong, D. Cheng, L. Liu, F. Chen, X. Zhan, Catal. Letters. 114 (2007) 198–201.

[157] H.-Z. Zhu, Y.-M. Lu, F.-J. Fan, S.-H. Yu, Nanoscale. 5 (2013) 7219–23.

[158] M. Badlani, I.E. Wachs, Catal. Letters. 75 (2001) 137–149.

[159] D. Kulkarni, I.E. Wachs, Appl. Catal. A Gen. 237 (2002) 121–137.

[160] M. Capdevila-Cortada, M. García-Melchor, N. López, J. Catal. 327 (2015) 58–64.

[161] L. Zhang, Z. Wu, N.C. Nelson, A.D. Sadow, I.I. Slowing, S.H. Overbury, ACS Catal. (2015) 6426–6435.

[162] M.A. Pacheco, C.L. Marshall, Energy & Fuels. 11 (1997) 2–29.

[163] P. Tundo, M. Selva, Acc. Chem. Res. 35 (2002) 706–716.

[164] M. Aresta, A. Dibenedetto, Dalton Trans. (2007) 2975–92.